



**HAL**  
open science

## Distribution and stability of Mn complexes in the ocean: Influence of hydrothermal plumes and weather events

Aubin Thibault de Chanvalon, George Luther, Véronique Oldham, Bradley Tebo, Nicole Coffey, Timothy Shaw

### ► To cite this version:

Aubin Thibault de Chanvalon, George Luther, Véronique Oldham, Bradley Tebo, Nicole Coffey, et al.. Distribution and stability of Mn complexes in the ocean: Influence of hydrothermal plumes and weather events. *Limnology and Oceanography*, 2023, 68 (2), pp.455-466. 10.1002/lno.12285 . hal-04284845

**HAL Id: hal-04284845**

**<https://hal.science/hal-04284845>**

Submitted on 14 Nov 2023

**HAL** is a multi-disciplinary open access archive for the deposit and dissemination of scientific research documents, whether they are published or not. The documents may come from teaching and research institutions in France or abroad, or from public or private research centers.

L'archive ouverte pluridisciplinaire **HAL**, est destinée au dépôt et à la diffusion de documents scientifiques de niveau recherche, publiés ou non, émanant des établissements d'enseignement et de recherche français ou étrangers, des laboratoires publics ou privés.

1       **Distribution and stability of Mn complexes in**  
2       **the ocean: influence of hydrothermal plumes**  
3       **and weather events.**

4       Aubin Thibault de Chanvalon<sup>1,2\*</sup>, [aubin.thibault-de-chanvalon@univ-pau.fr](mailto:aubin.thibault-de-chanvalon@univ-pau.fr) <sup>1</sup>University of  
5       Delaware School of Marine Science & Policy, 700 Pilottown Road, Lewes, DE, 19958, USA  
6       <sup>2</sup>CNRS, Universite de Pau et des Pays de l'Adour, E2S UPPA, IPREM, UMR 5254, Pau, France

7       George W. Luther III<sup>1</sup>, [luther@udel.edu](mailto:luther@udel.edu) <sup>1</sup>University of Delaware School of Marine Science &  
8       Policy, 700 Pilottown Road, Lewes, DE, 19958, USA

9       Véronique E. Oldham<sup>1,3</sup>, [voldham@uri.edu](mailto:voldham@uri.edu) <sup>1</sup>University of Delaware College of Earth, Ocean,  
10       and Environment, 700 Pilottown Road, Lewes, DE, 19958, USA, <sup>3</sup>University of Rhode Island,  
11       Graduate School of Oceanography, 215 S Ferry Lane, Narragansett, RI, 02882, USA

12       Bradley M. Tebo<sup>4</sup>, [tebob@ohsu.edu](mailto:tebob@ohsu.edu), <sup>4</sup>Oregon Health & Science University, Portland, OR,  
13       97239, USA. Current address: University of Washington, Seattle, WA 98195

14       Nicole R. Coffey<sup>1,6</sup>, [coffeyni@oregonstate.edu](mailto:coffeyni@oregonstate.edu), <sup>6</sup>Oregon State University, College of Earth,  
15       Ocean, and Atmospheric Sciences, Corvallis, OR, 97331-4501, USA

16       Timothy F. Shaw<sup>5</sup>, [SHAW@mailbox.sc.edu](mailto:SHAW@mailbox.sc.edu), <sup>5</sup>University of South Carolina, Columbia, SC,  
17       29208, USA

18       **Key words:** Manganese; metal speciation; Oxygen minimum zone; biogeochemistry;  
19       hydrothermal plume; complexes stability;

20       **Running head:** Stability of Mn complexes in ocean

22  
23  
24  
25  
26  
27  
28  
29  
30  
31  
32  
33  
34

## **Abstract**

We measured the speciation of dissolved Mn from the surface to just above the hydrothermal vents at 9°50'N East Pacific Rise in the open ocean of the Pacific over a three week period. Total dissolved Mn concentrations ranged from 2.2 to 135 nM with a significant contribution of dissolved Mn(III) bound to humic acid in one third of our samples representing up to 64% of the total dissolved Mn. These humic complexes were mostly detected in the hydrothermal vent plume and at the redox boundaries of the oxygen minimum zone in the water column. In the hydrothermal plume, the Mn(III)-humic acid stabilized the manganese in solution up to a ~10,000-fold dilution of the venting water. In the upper water column, Mn(III)-humic acid was only detected after a squall and rain event, which indicates that it is a transient species, persistent over days to weeks. This temporal variability highlights the importance of non-steady-state processes in the open ocean, which may help to explain previous observations of a dissolved Mn maximum within oceanic oxygen minimum zones.

## Introduction

35  
36  
37 The vertical distribution of total dissolved manganese in the East Pacific margin is usually  
38 depicted with three concentration maxima: at the surface, in the oxygen minimum zone and, where  
39 present, in hydrothermal vent plumes (*e.g.* Klinkhammer and Bender 1980; Martin et al. 1985;  
40 Resing et al. 2015). For the first maximum at the surface, the principal source of dissolved Mn is  
41 atmospheric dust deposition dissolved by photoreduction (*e.g.* Guieu et al., 1994; Mendez et al.,  
42 2010; Sunda et al., 1983) and, of lower magnitude, by efflux of dissolved Mn(II) from coastal  
43 sediment (*e.g.* McManus et al., 2012). Sunda and Huntsman (1988) showed that high surface  
44 dissolved Mn concentration is also maintained due to photoinhibition of biological Mn oxide  
45 formation. In the surface ocean maximum, the removal of dissolved Mn occurs primarily via  
46 biological uptake, adsorption onto particles and abiotic and biotic oxidation to solid Mn(III/IV)  
47 oxides (Sunda and Huntsman 1990).

48 In the oxygen minimum zone, several Mn sources have been considered for the second dissolved  
49 Mn maximum, fueling a debate between three models explaining the dissolved Mn maximum  
50 (Klinkhammer and Bender 1980): model A, the dissolution of Mn oxides in the oxygen minimum  
51 zone due to the *in situ* low dissolved oxygen/low pH (Klinkhammer and Bender 1980; Lam et al.  
52 2018); model B, the offshore transport of sediment porewater efflux favored by the slow oxidation  
53 kinetics of Mn(II) in the oxygen minimum zone (*e.g.* Martin and Knauer 1984; Lewis and Luther  
54 III 2000; Cutter et al. 2018); and model C, the release of dissolved Mn by mineralization of organic  
55 matter (Johnson et al. 1996; Vedamati et al. 2015; Sanial et al. 2017). There are two common  
56 assumptions regarding Mn redox chemistry within these three models. First, they assume that the  
57 total dissolved Mn pool is comprised of only Mn(II), whereas recently, much work has reported on

58 the environmental importance of dissolved Mn(III) bound to organic ligands (*e.g.* Trouwborst et  
59 al. 2006; Madison et al. 2011; Jones et al. 2020) and laboratory results have shown that certain  
60 organic and inorganic ligands prevent dissolved Mn(III) disproportionation for weeks (*e.g.* Kostka  
61 et al., 1995). However, these prior field studies have only examined estuarine water columns and  
62 sediment porewaters, with dissolved Mn concentration exceeding 20 nM. More recent  
63 investigations on the continental shelf of the Northwest Atlantic ocean (Oldham et al. 2020) and  
64 into the open ocean waters of the Northwest Atlantic Ocean (Jones et al. 2020) report important  
65 contributions of Mn(III) to the total dissolved Mn pool, though decreasing offshore. Jones et al  
66 (2020) report increased contributions of Mn(III) in the oxygen minimum zone waters that have a  
67 O<sub>2</sub> saturation state of 50%. The first goal of the present study is thus to determine whether Mn(III)  
68 is an important component of the total dissolved Mn pool in the open ocean system of the Pacific.

69 The second assumption of the above models is that they assume the system is at steady state.  
70 Sampling during cruises doing transects with short stops on each station favors the interpretation  
71 of changes due to vertical and lateral heterogeneity rather than temporal variation. However, storms  
72 and/or eddies are known to change, sometimes drastically, the water column properties (*e.g.* Babin  
73 et al., 2004). This could be especially important for metastable species, such as dissolved Mn(III),  
74 since its stability depends on the complex(es) it forms. Thus, our second goal is to address this  
75 potential for temporal variability in the stabilization of dissolved Mn(III); to this aim, we sampled  
76 the water column over the course of three weeks at the same station above the East Pacific Rise  
77 hydrothermal vent system, 900 km south of Mexico and 2000 km west of Costa Rica.

78 In the deep ocean, the third dissolved Mn maximum is a well-known feature of active  
79 hydrothermal sources which release dissolved Mn suspected to be Mn(II) (*e.g.* Klinkhammer et al.,  
80 1977). This dissolved Mn can be transported vertically several hundred meters above the vent

81 source and can also be transported laterally hundreds to thousands of kilometers (Fitzsimmons et  
82 al. 2014). Possible removal processes from vent sources include bacterial dissolved Mn(II)  
83 oxidation in the vent water (Ehrlich, 1983; Dick et al., 2006; Mandernack and Tebo, 1993) and in  
84 the plume (Cowen et al. 1986), as well as abiotic dissolved Mn(II) oxidation and/or adsorption onto  
85 particles (Mandernack and Tebo 1993). Therefore, the third goal of our work is to characterize the  
86 importance of organic ligands capable of stabilizing dissolved Mn(III) in the East Pacific Rise  
87 (EPR) hydrothermal plume. The vent work reported here builds on the chemistry that our group  
88 (Shaw et al, 2021) found in the dynamic mixing zone from the vent orifice to about 3 meters above  
89 the vent, which is the origin of the vent plume. In Shaw et al (2021), we showed that dissolved  
90 Mn(III) was produced due to the formation of reactive oxygen species as the thermodynamics of  
91 Mn(II) oxidation by O<sub>2</sub> is not favorable (Luther, 2010). Here, we show that dissolved Mn(III)  
92 formed in the dynamic mixing zone is transported in the resulting plume into the water column.

93 Overall, this study tries to answer A) Is Mn(III)-ligand an important component of the total  
94 dissolved Mn pool in the open ocean ? B) How does temporal variability affect the distribution of  
95 Mn(III)-ligand ? and C) Is Mn stabilized as a complex by organic ligand in the vent plume?

## Materials and methods

### Seawater sampling

Four vertical water column profiles of chemical and physical properties were performed at 9° 50' N East Pacific Rise (104° 17' W) on April 3, 6, 13 and 15 of 2017 aboard the R/V *Atlantis*. A squall, with average wind speed of 40 km h<sup>-1</sup> associated with 10 mm of rain, occurred on April 11th and 12th, 2017. During each cast, 12 depths were sampled in duplicate using a 24-Niskin bottle rosette equipped with a Seabird 911 CTD (Conductivity, Temperature, Depth) profiler as well as oxygen (SBE43), fluorescence (Wetlabs FLNTURTD) and beam transmission (Wetlabs C-Star transmissometer) sensors. The Oxygen sensor has a reported detection limit of 3 μM with high stability (shift < 1 μM/month). As our profiles occurred over a 12-day period and the O<sub>2</sub> concentration difference before and after the squalls was > 2 μM, we regard comparisons at low O<sub>2</sub> concentrations as reliable because of the sensor's high stability. In addition to these sensors, a transponder was put on the CTD rosette to communicate with a deep ocean transponder placed via the HOV *Alvin* so that the rising plume could be better detected, and samples could be obtained closer to the source hydrothermal vents. The transponder allowed us to sample in or nearer the vent plume than could be done in other work (e.g., Fitzsimmons et al 2017; Lam et al, 2018).

The sampling was focused above, within and below the oxygen minimum zone and, in particular, along the oxygen decrease from the surface to the top of the oxygen minimum zone, as determined by the *in situ* dissolved oxygen profile. Water samples were obtained thanks to 10-liter external spring trace metal Niskin bottles by General Oceanics, acid cleaned on deck prior to deployment. Blanks showed negligible Mn contamination. Two liters aliquots were collected using acid-washed tubing into acid-washed LDPE bottles after triplicate rinsing, and minimizing atmospheric oxygen

118 contamination by overflowing bottles. Samples were filtered by vacuum pump within 1 hour of  
119 collection through 47 mm diameter 0.2  $\mu\text{m}$  acid cleaned membrane filters (polycarbonate from  
120 Whatman®, in a  $\text{N}_2$ -filled glove bag for oxygen minimum zone samples) using acid-cleaned  
121 polycarbonate filtration units (Savillex). Filtered samples were not acidified but frozen and  
122 preserved at  $-20^\circ\text{C}$  until analysis.

### 123 **Dissolved Mn speciation measurements**

124 Dissolved Mn speciation was measured by UV-vis adsorption at 468 nm of a Mn-porphyrin  
125 complex formed after a Cd(II)-porphyrin reagent addition to the sample (Ishii et al. 1982). Details  
126 of the method are described in Thibault de Chanvalon and Luther 2019. The final concentrations  
127 of the Cd(II)-porphyrin reagent components after mixing with the sample are: sodium tetraborate  
128 ( $500\ \mu\text{M}$ ), imidazole (18 mM), T(4-CP)P porphyrin (240 nM) and  $\text{CdCl}_2$  (24  $\mu\text{M}$ ). The UV-vis  
129 adsorption was measured in a 500-cm long wave capillary cell (World Precision Instrument) which  
130 gives a detection limit of 0.3 nM (3x times the blank's standard deviation). Three discrete aliquots  
131 of a sample are measured in triplicate (Table 1). These aliquots divide the total dissolved Mn pool  
132 into three conceptual fractions in Table 1 (dissolved Mn(II); dissolved Mn(II) and Mn(III)-humic  
133 acid; total dissolved Mn), which are distinguishable by the chemical properties of each fraction.

134 The “heated only” aliquot corresponds to the measurement after 60 minutes of reacting in a 90  
135  $^\circ\text{C}$  water bath and corresponds to the complexation of Mn(II) and any weak and fast reacting  
136 Mn(III) complexes. For simplicity, we refer to this fraction as Mn(II) even if it includes some  
137 Mn(III)-ligand<sub>weak</sub> ( $\log K_{\text{cond}} < 11.6$ ) described previously (Madison et al. 2011).

138 The “HA removed” aliquot is acidified ( $\text{pH} < 2$ ) and filtered prior to the reagent addition and  
139 similar heating and causes removal of the associated Mn (Oldham et al., 2017a,b). Since Mn(II)



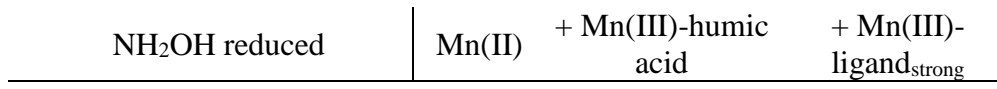
140 binds very weakly to organic matter (Irving and Williams 1948; Madison et al. 2011), we assume  
 141 that the Mn precipitating with humic materials is Mn(III) (Mn(III)-humic acid). The Mn remaining  
 142 in solution after acid precipitation is Mn(II). Thus, the difference between dissolved Mn in the  
 143 heated fraction and the Mn(II) in the solution after acid precipitation of humic acids provides the  
 144 concentration of Mn(III)-humic acid. We note that humic material in waters near vents can come  
 145 from several sources including the vents, chemosynthetic organisms surrounding vents and bottom  
 146 waters; functional groups include hydroxylated aromatic and nonaromatic compounds that can bind  
 147 metals (Luther 2021).

148 Finally, the “NH<sub>2</sub>OH reduced” aliquot is treated with a strong reducing agent, NH<sub>2</sub>OH (final  
 149 concentration of 100 nM), to reduce all Mn(III)-ligand compounds to Mn(II) before addition of the  
 150 Cd(II)-porphyrin reagent and heating. In this latter case, both Mn(II), Mn(III)-humic acid and any  
 151 manganese bound to a strong ligand (Mn(III)-ligand<sub>strong</sub>) are complexed by the Cd(II)-porphyrin  
 152 reagent. This measurement gives the total dissolved Mn concentration.

153 In Thibault de Chanvalon and Luther (2019), we reported that the method agrees with other  
 154 methods on known standards. We measured total manganese [after the heating treatment (Mn(II)+  
 155 Mn(III)-ligand<sub>weak</sub> + Mn(III)-humic acid)] using the Canadian NASS-6 standard material at  $10.1 \pm$   
 156  $0.7$  nM (n=12, consensus NASS value of  $9.65 \pm 0.92$  nM) and in the Geotracas SAFe-S material at  
 157  $0.82 \pm 0.17$  nM (n=9, consensus SAFe-S value of  $0.825 \pm 0.08$  nM).

158 Table 1: correspondence between analyses and expected speciation measured

Dissolved Mn Analyses	Expected speciation measured
HA removed	Mn(II)
Heated only	Mn(II) + Mn(III)-humic acid



160

# Results

161

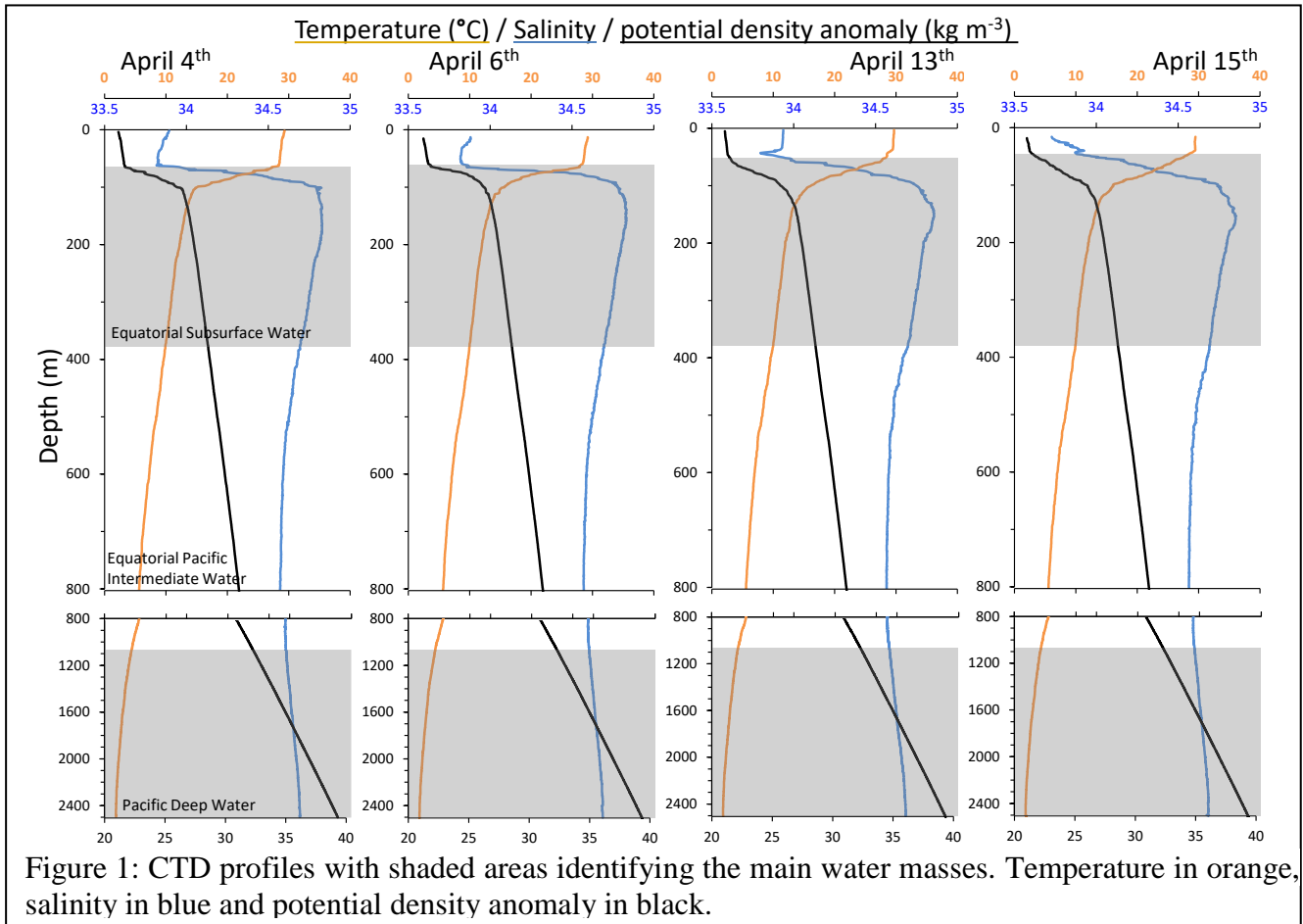
## CTD data and identification of water masses

162

The salinity and temperature profiles of the water column (Figure 1) permit identification of 4

163

main water masses.



164

(1) The surface layer ( $21 < \sigma_\theta$  (potential density anomaly)  $< 21.6$ ) with low salinity, high

165

temperature and high oxygen concentration, extended from the surface down to  $65 \pm 5$  m

166

depth. This depth also corresponded to the fluorescence maximum and to the beam

167

transmission minimum (Figure 2). The squall (11<sup>th</sup> and 12<sup>th</sup> April) impacted the water column

168

properties and raised the start of the dissolved oxygen gradient from 68 to 55 m depth (Figure

169

3A). However, these depths corresponded to an identical potential density ( $\sigma_\theta = 21.6$ ), which

170 indicates that the elevation of the oxygen gradient is produced by an increase of mixing  
 171 between the surface layer and the layer beneath.

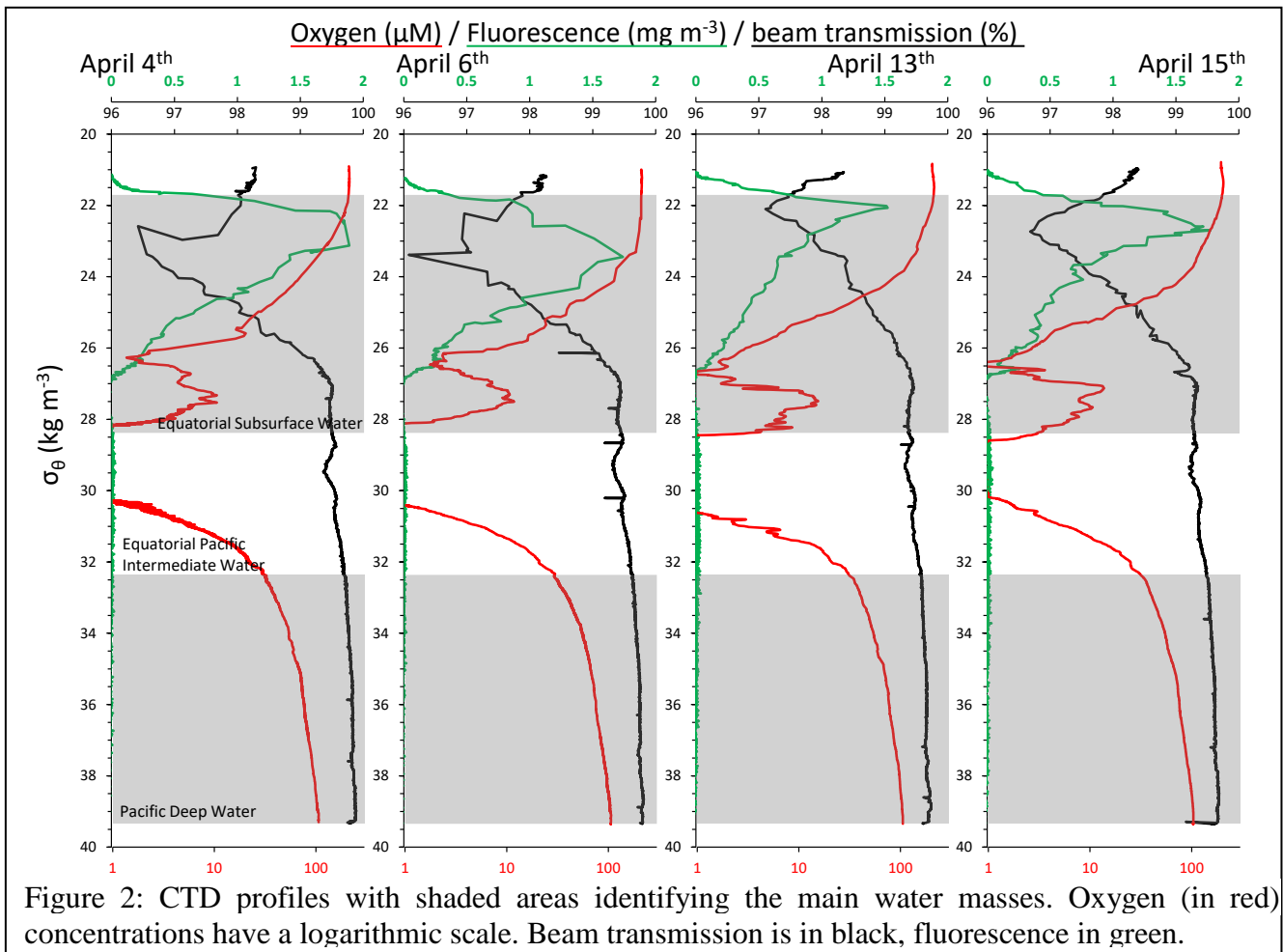
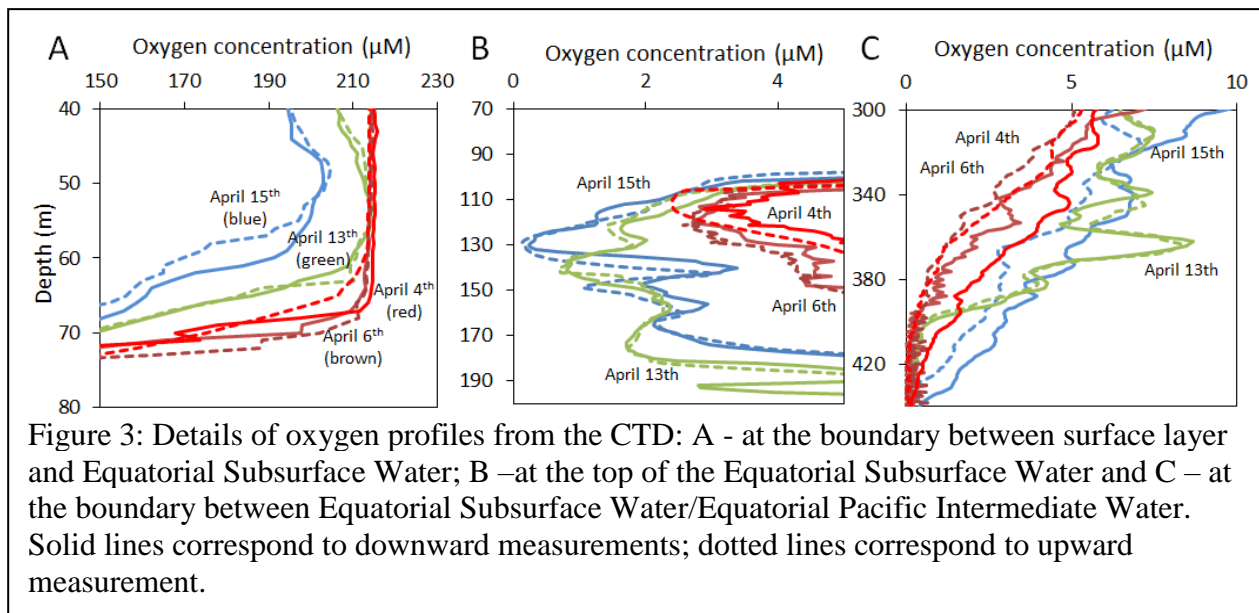


Figure 2: CTD profiles with shaded areas identifying the main water masses. Oxygen (in red) concentrations have a logarithmic scale. Beam transmission is in black, fluorescence in green.

172 (2) The Equatorial Subsurface Water (Peters et al., 2017) between ~ 70 m and ~ 400 m depth  
 173 ( $21.6 < \sigma_{\theta} < 28.4$ ) is characterized by high salinity and an oxygen concentration that drops sharply,  
 174 reaches a first minimum at  $\sigma_{\theta} = 26.6$ , then varies between  $1 \mu\text{M}$  and  $15 \mu\text{M}$  (Figure 2). In this layer,  
 175 the impact of the squall is visible on the oxygen minimum of the Equatorial Subsurface Water that  
 176 decreases from  $3 \mu\text{M}$  to  $< 1 \mu\text{M}$  at 120 m depth (Figure 3B). Moreover, at the lower Equatorial  
 177 Subsurface Water limit (~ 400m depth), the weakly oxygenated water (between  $1 \mu\text{M}$  and  $15 \mu\text{M}$ )  
 178 expands downward after the squall (Figure 3C) suggesting a possible increase of water mixing  
 179 down to this depth.



180 (3) The Equatorial Pacific Intermediate Water (Figure 1), between ~ 400 m and ~ 1100 m depth  
 181 ( $28.4 < \sigma_{\theta} < 32.4$ ), is characterized by an oxygen depletion with concentration mostly below the  
 182 sensor’s detection limit of  $3 \mu\text{M}$ . Two weak beam transmission maxima are constant over time at  
 183  $\sigma_{\theta} = 29.5$  and  $\sigma_{\theta} = 30.6$  (Figure 2).

184 Below the Equatorial Pacific Intermediate Water is the (4) Pacific Deep Water, with density  
 185 above  $\sigma_{\theta} = 32.4$ . This zone is characterized by low temperature and high concentrations of oxygen.  
 186 Close to the bottom (at 2500 m depth), a decrease of beam transmission was observed on the 4<sup>th</sup>,  
 187 13<sup>th</sup> and 15<sup>th</sup> April because the CTD was in the plume produced by the active vents of the East  
 188 Pacific Rise.

### 189 **Manganese speciation**

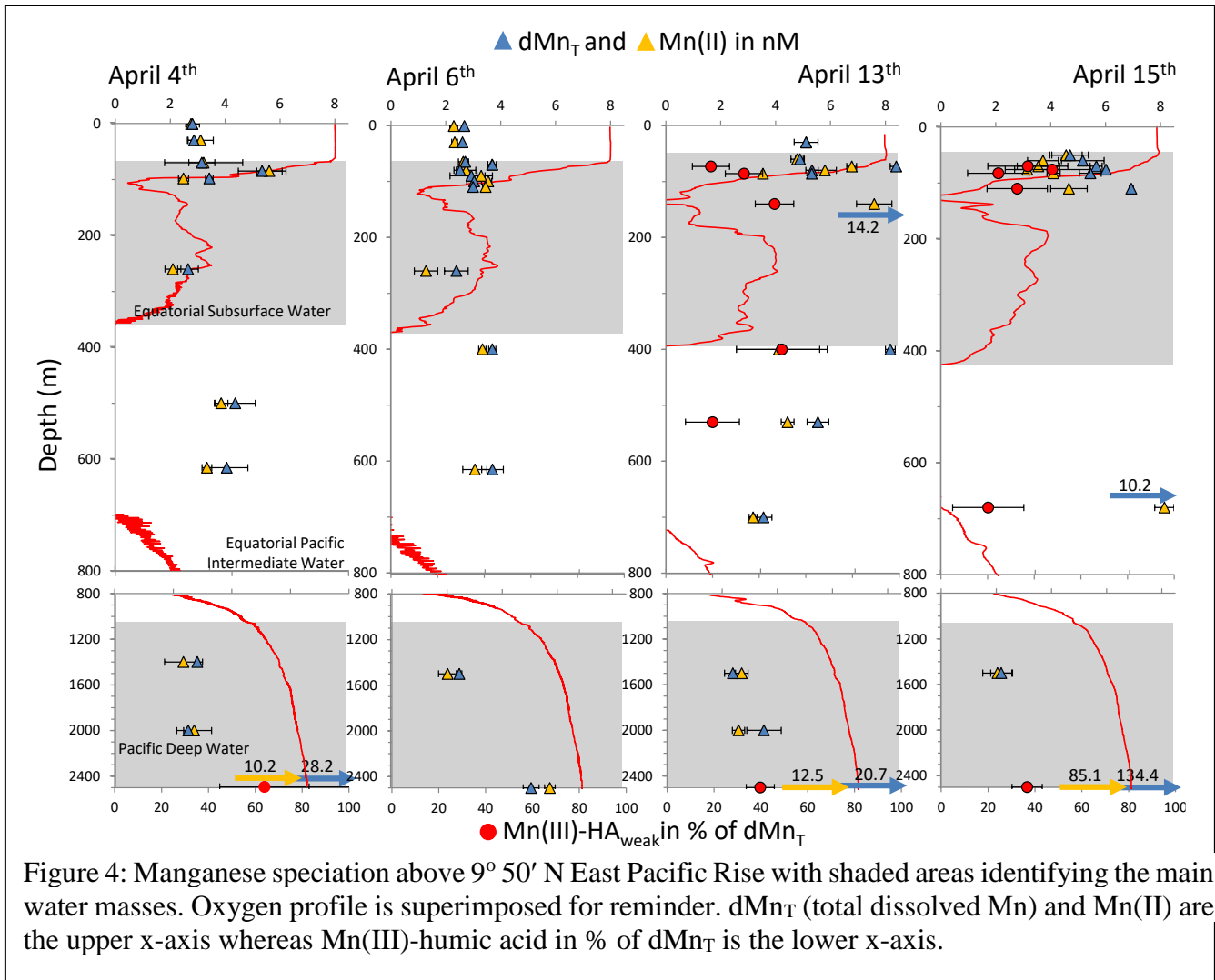
190 The manganese concentrations obtained with the methods “heated only” and “ $\text{NH}_2\text{OH}$  reduced”  
 191 show similar results (Table 2). According to the operational definitions from Table 1, this indicates  
 192 that there is no  $\text{Mn(III)-ligand}_{\text{strong}}$  present in our samples. Because of these similarities, we describe  
 193 total dissolved Mn using the results from the “heated only” method. In contrast, the results from

194 the acidified, “HA removed” method showed lower dissolved Mn values than the non-acidified  
 195 method in 31% of the samples, indicating Mn removal during the acidification step. Mn is likely  
 196 to be removed during the acidification if it is bound to humic material, which precipitates at  $\text{pH} < 2$ ,  
 197 and if it is not dissociated from its ligand (Oldham et al., 2017a,b). Therefore, the Mn(III)-humic  
 198 acid is calculated by difference between the “heated only” and “HA removed” methods (Table 1).

199 Table 2: Slope (a) and correlation coefficient between the concentrations  
 200 measured with the methods “heated only” and “NH<sub>2</sub>OH reduced”

Date	“heated only” versus “NH <sub>2</sub> OH reduced”
April 4 <sup>th</sup>	a = 1.01 r <sup>2</sup> = 0.82
April 6 <sup>th</sup>	a = 1.00 r <sup>2</sup> = 0.72
April 13 <sup>th</sup>	no data
April 15 <sup>th</sup>	no data

201 The concentrations of total dissolved Mn before the squall (4<sup>th</sup> and 6<sup>th</sup> April, Figure 4 and  
 202 Supporting Information Table S1) correspond to previous manganese profiles from this region  
 203 (Klinkhammer and Bender 1980; Murray et al. 1983) with surface concentrations between 2.6 and  
 204 2.9 nM. A second maximum occurs at the oxycline, with values of 5.3 and 3.7 nM for April 4<sup>th</sup> and  
 205 6<sup>th</sup>, followed by a decrease in the Equatorial Subsurface Water (total dissolved Mn = 2.6 and 2.4  
 206 nM). A third maximum is visible in the center of the oxygen minimum zone (4.4 and 3.7 nM for  
 207 April 4<sup>th</sup> and 6<sup>th</sup>) and lower concentrations (2.3 nM) are observed in the Pacific Deep Water at 1500  
 208 m depth. No Mn(III)-humic acid complexes were detected in the water column before the squall  
 209 with the exception of above the hydrothermal vent.



210 After the squall, the total dissolved Mn concentrations increased at the surface (Figure 4, April  
 211 13<sup>th</sup> and 15<sup>th</sup>) up to 5 nM (at 30 m depth), likely due to the dissolution of dust deposition associated  
 212 with the rain event, but no form of dissolved Mn(III) was identified. Although we have no data  
 213 from aerosol samples, Marsay et al. (2022) and Buck et al. (2019) show that Mn from crustal  
 214 sources is present in dust samples from the Eastern and Central Pacific, respectively, indicating  
 215 that Mn was deposited to our surface waters after the rain event.

216 At the oxycline, total dissolved Mn concentration increased after the squall up to 8.4 nM and was  
 217 composed of, on average, 33% Mn(III)-humic acid (Table 3). At 140 m depth, in the Equatorial

218 Subsurface Water, a particularly high total dissolved Mn concentrations (14.2 nM) associated with  
 219 the detection of Mn(III)-humic acid was also observed and coincided with an oxygen decrease  
 220 during the squall (from 3  $\mu$ M to < 1  $\mu$ M, Figure 3B). Finally, at the boundaries of the oxygen  
 221 minimum zone (400 and 680 m depth), an increase of total dissolved Mn (up to 8.1 nM at 400m  
 222 depth and 10.2 nM at 680 m depth) associated with Mn(III)-humic acid is observed after the squall.

223 Table 3: Beam transmission and temperature signature of bottom water (depth = 2504  $\pm$  6 m)  
 224 compared to the manganese speciation. The dilution factor is calculated based on the bottom water  
 225 change of Temperature compared to the measured temperature of the closest venting water.

Date	Location	Closest vent	Bottom change of beam transmission	Bottom change of Temperature ( $^{\circ}$ C)	Temperature of venting water ( $^{\circ}$ C)	total dissolved Mn (nM)	Mn(III)-humic acid (% total dissolved Mn)	Dilution factor
April 4 <sup>th</sup>	9 <sup>o</sup> 50.97N 104 <sup>o</sup> 17.62W	BioVent	-0.13 %	+0.05	310	28.2	64	5740
April 6 <sup>th</sup>	9 <sup>o</sup> 47.25N 104 <sup>o</sup> 16.97W	V Vent	0.0 %	0.0	ND	5	0	>20000
April 13 <sup>th</sup>	9 <sup>o</sup> 50.31N 104 <sup>o</sup> 17.48W	Bio 9 Vent	-0.08 %	+0.04	370	20.7	40	9250
April 15 <sup>th</sup>	9 <sup>o</sup> 50.15N 104 <sup>o</sup> 17.46W	P Vent	-0.7 %	+0.13	360	134.4	37	2950

226  
 227 Above the hydrothermal vents (~10 m), the beam transmission shows attenuation on April 4<sup>th</sup>,  
 228 13<sup>th</sup> and 15<sup>th</sup> due to the particles carried by the vent plume (Figure 2) while the temperature  
 229 increases. The bottom changes of both temperature and beam transmission were obtained from a  
 230 close look at the data from the ten deepest meters obtained during the CTD casts (Supporting  
 231 Information Fig. S1). Table 3 shows the strong relationship between the bottom changes of beam  
 232 transmission and temperature increases ( $r^2 > 0.9$ ) along with an increase in dissolved Mn, indicating  
 233 that vent fluid emission is the major source of dissolved Mn in this system. In particular, Figure 5  
 234 shows that Mn(III)-humic acid increase linearly with temperature anomalies with a slope of 320  $\pm$   
 235 100 nM  $^{\circ}$ C<sup>-1</sup> and account for 37 - 64% of total dissolved Mn while dissolved Mn(II) presents an



236 important loss between temperature anomalies of 0.13 °C and 0.05 °C. In contrast, on the 6<sup>th</sup> of  
237 April, we did not detect a plume (no beam transmission nor temperature anomaly) and there were  
238 lower total dissolved Mn concentrations (5 nM) and no detectable Mn(III)-humic acid.

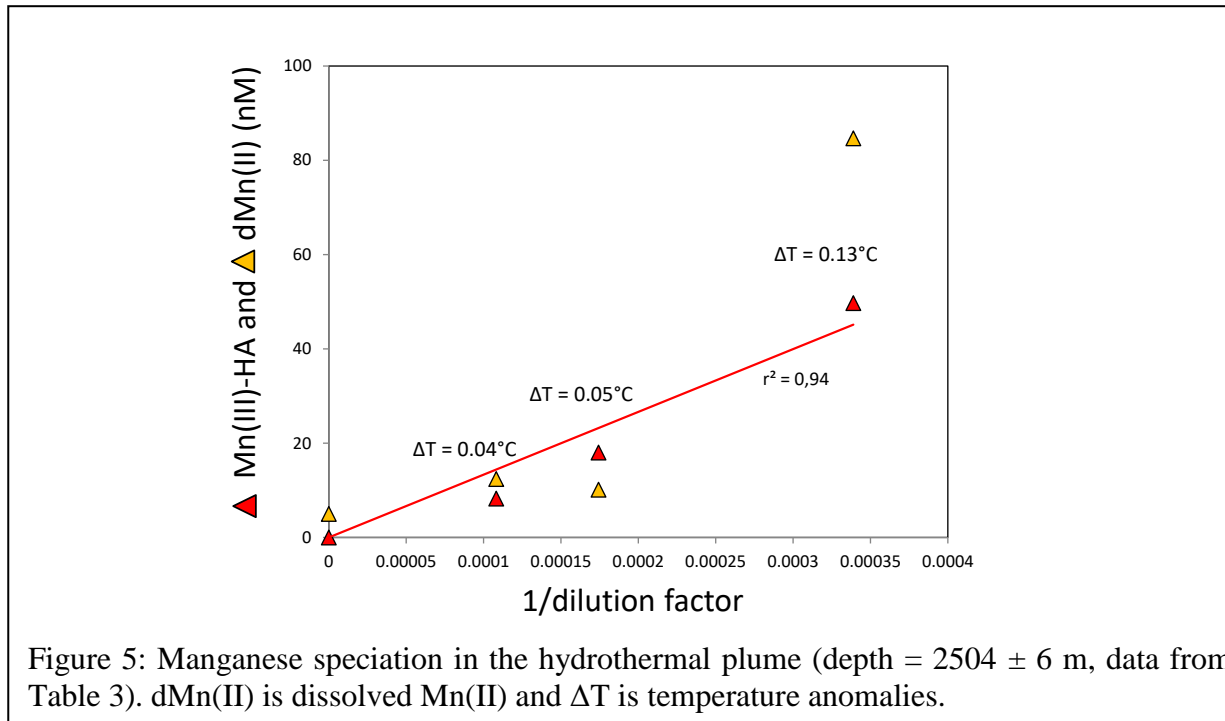


Figure 5: Manganese speciation in the hydrothermal plume (depth =  $2504 \pm 6$  m, data from Table 3). dMn(II) is dissolved Mn(II) and  $\Delta T$  is temperature anomalies.

239

240

## Discussion

241  
242 On April 11th and 12th, a squall with average wind speed of 40 km h<sup>-1</sup> and a rainfall of 10 mm  
243 occurs simultaneously to significant water mixing. At redox gradient depths, after the squall, an  
244 important increase of total dissolved Mn was observed, in association with dissolved Mn(III). The  
245 three first parts of the discussion propose explanations for these changes comparing the situation  
246 before to the situation after the squall. The last part of the discussion focuses on the role of  
247 hydrothermal vents whose plume was always associated with important Mn (III) contribution.

### Mn speciation before the squall (surface and Oxygen minimum zone)

248  
249 For the April 4<sup>th</sup> and 6<sup>th</sup> samplings, dissolved Mn speciation indicates that only dissolved Mn(II)  
250 is detected except above the hydrothermal vent on April 4 (Table S1). April 4<sup>th</sup> and 6<sup>th</sup> dissolved  
251 Mn profiles (Figure 4) present the typical features across the oxygen minimum zone including a  
252 sharp peak of total dissolved Mn concentration at the oxycline up to 5.3 nM, as recently observed  
253 in other oxygen minimum zones (Vedamati et al. 2015; Sanial et al. 2017) and a broader increase  
254 of total dissolved Mn (up to 4.4 nM) in the core of the oxygen minimum zone reported in this  
255 region since the 1980s (Klinkhammer and Bender 1980; Martin and Knauer 1984). Three models  
256 can independently explain these observations alone or in combination: the dissolution of Mn oxides  
257 settling from the mixed layer (model A, Klinkhammer and Bender, 1980; Lam et al., 2017); the  
258 offshore transport of sedimentary efflux in a context of slow dissolved Mn removal by reoxidation  
259 due to the oxygen minimum zone (model B, Martin and Knauer, 1984; Lewis and Luther III, 2000;  
260 Cutter et al., 2018) or the *in situ* mineralization of organic matter associated also with slow  
261 oxidation (model C, Johnson et al., 1996; Vedamati et al., 2015; Sanial et al., 2017). The absence  
262 of measurable dissolved Mn(III) on April 4<sup>th</sup> and 6<sup>th</sup> samples bring new information of the ongoing  
263 processes. Indeed, previous studies over a natural redox gradient in the Black Sea (Trouwborst et

264 al. 2006; Yakushev et al. 2009), estuaries (Oldham et al. 2017b; a; Jones et al. 2019) and porewaters  
265 (Madison et al. 2013) demonstrate the ubiquity of dissolved Mn(III) where intense redox reactions  
266 occur. The production of dissolved Mn(III) during Mn oxide reduction is further supported by  
267 laboratory experiments (Stone 1987; Perez-Benito 2002) including electrochemical (Ruppel et al.  
268 2001), ligand driven (Duckworth and Sposito 2007) and bacterial reduction (Lin et al. 2012).  
269 Finally, thermodynamic considerations also highlight the efficiency of two one-electron transfer  
270 steps versus a single two-electron step (Luther 2005; Luther et al. 2018) which also supports the  
271 formation of intermediate Mn(III) during redox reactions. Thus, the absence of dissolved Mn(III)  
272 before the squall (on April 4<sup>th</sup> and 6<sup>th</sup> samples; Figure 4) implicates a weak intensity of redox  
273 reactions such as Mn(IV) oxide reduction to dissolved Mn(II) which favors models B or C over  
274 model A.

#### 275 **Mn speciation after the squall (surface and Oxygen minimum zone)**

276 After the squall (on April 13<sup>th</sup> and 15<sup>th</sup>), changes of temperature, salinity and oxygen gradient  
277 (Figure 1, Figure 2 and Figure 3A) indicate important mixing between the oxygenated mixed layer  
278 and the low oxygenated Equatorial Subsurface Water that would stimulate redox reactions. The  
279 notable increase of total dissolved Mn (Figure 4, April 13<sup>th</sup> and 15<sup>th</sup>) indicates new atmospheric  
280 input of manganese in the water column while the appearance of Mn(III)-humic acid suggests  
281 significant redox recycling. A significant wet deposition of Mn during the squall followed by the  
282 reductive dissolution of Mn(III/IV) oxides can explain these observations (model A). The models  
283 B and C are not likely since there is no indication of an increase of transport rate of the sedimentary  
284 efflux (model B) nor an increase of organic matter degradation (model C). Contrastingly, oxide  
285 reduction is supported by the presence of sufficient reductants in the top of the east Pacific oxygen  
286 minimum zone (*e.g.* Vedamati et al., 2015; Cutter et al., 2018) such as Fe<sup>2+</sup> (Hartman et al. 1984;

287 Van Cappellen and Wang 1996), NH<sub>3</sub> (Luther et al. 1997), dissolved organic matter (Stone and  
288 Morgan 1984) or NO<sub>2</sub><sup>-</sup> (Bartlett 1981; Lewis and Luther III 2000). Additionally, the reducing  
289 conditions in the upper oxygen minimum zone are reinforced after the mixing event with an oxygen  
290 concentration that decreases (Figure 3B). However, the wet dust input is probably limited to the  
291 top of the oxygen minimum zone while, in our dataset, some increase of total dissolved Mn and  
292 Mn(III)-humic acid is also found at 400 and at 700 m depths, with concentrations reaching up to  
293 8.2 nM and 10.2 nM respectively. These latter data suggest the occurrence of another source of  
294 manganese oxides that are mixed and reduced within the oxygen minimum zone during the squall.  
295 Contamination is unlikely since these two data points were processed simultaneously with other  
296 samples, and, in addition, samples from two different Niskin bottles from each depth show  
297 consistency. While surprising, these high values could be explained by the reduction of subsurface  
298 Mn oxides transported by horizontal eddies, which are very common in this region (Kessler 2006;  
299 Cole et al. 2015).

### 300 **Lifetime of Mn(III)-humic acid in the oxygen minimum zone**

301 The lifetime of Mn(III)-humic acid depends on the properties of the humic ligands that stabilize  
302 Mn(III). At our site, the lifetime of Mn(III)-humic acid is longer than 3 days (the time between the  
303 squall and our measurements) and is shorter than the delay since the last squall, probably about one  
304 month, as Mn(III)-humic acid was not observed before the squall. This lifetime may limit the role  
305 of Mn(III)-humic acid ligands in stabilizing dissolved Mn during long-term transport. Additionally,  
306 the Mn(III)-humic acid is recovered in both the “NH<sub>2</sub>OH reduced” and the “heated only” aliquots,  
307 which indicates a quite rapid dissociation constant ( $k_d > 2.8 \times 10^{-4} \text{ s}^{-1}$ ; Luther et al. 2015 ). If we  
308 assume a formation constant ( $k_f$ ) equal to  $10^9 \text{ M}^{-1} \text{ s}^{-1}$ , as in Luther et al. (2015), it corresponds to a  
309 stability constant  $K_{\text{COND}}=k_f/k_d$  inferior to  $10^{12.6}$ . This weak complexation of the HA ligands

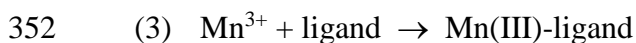
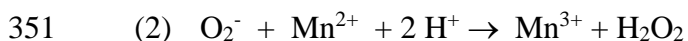
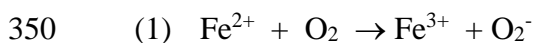
310 corresponds to the findings of Oldham et al. (2017b) in estuarine waters but contrasts with the St.  
311 Lawrence Estuary waters, where Oldham et al. (2017c) showed that Mn(III)-humic acid was  
312 included in the “NH<sub>2</sub>OH reduced” aliquots but not in the “heated only” aliquots. To sum up, the  
313 occurrence of a metastable redox state of dissolved Mn demonstrates the non-equilibrium state of  
314 Mn in the water column in proximity of important redox gradients, and highlights the importance  
315 of short-term temporal effects that impact Mn cycling after a storm event. Taking into account this  
316 variability, we suggest that offshore transport of sediment efflux or organic matter remineralization  
317 (model B and C) control the Mn concentration at the steady state, but that the redox dissolution  
318 becomes more important after mixing events (model A). These features are usually not described  
319 because most samples come from cruises that do not stay at the same location for more than one  
320 sampling.

### 321 **Impact of hydrothermal vents on dissolved Mn distribution**

322 The increase of dissolved Mn at the bottom of our water column profile, due to hydrothermal  
323 venting, is revealed by the increase of dissolved Mn concentration with temperature anomalies and  
324 increased particles as determined by transmissometer (Table 3). The temperature anomalies  
325 observed at 0.04, 0.05 and 0.13°C correspond to a vent water diluted 3,000 to 10,000-fold (Table  
326 3). Figure 5 shows that Mn(III)-humic acid behaves conservatively with a slope of  $320 \pm 100$  nM  
327 °C<sup>-1</sup>, indicating an absence of reaction in the plume between dilution 3,000 to dilution 10,000.  
328 Additionally, an extrapolation up to 28 °C gives a concentration of Mn(III)-humic acid of  $10 \pm 3$   
329 μM, which corresponds to the value measured independently for Mn(III) bound to a strong ligand,  
330 from a HOV *Alvin* dive sampling (Shaw et al. 2021) and suggests a continuous Mn(III) stabilization  
331 effect of ligands between dilution 10 and dilution 10,000. Thus, a significant quantity of dissolved  
332 Mn(III) is produced in proximity of the vent before the plume temperature decreases down to 28

333 °C (dilution 10), probably in few minutes. This formation can be explained by rapid dissolved  
334 Mn(II) oxidation in the presence of important humic like material produced by local bacterial and  
335 macrofaunal communities (Lang et al. 2006; Longnecker et al. 2018). These two groups showed  
336 that there is higher dissolved organic carbon of 5 μM to 14 μM in waters surrounding vents  
337 compared to the ambient deep seawater.

338 Conditions in the venting waters are acidic and O<sub>2</sub> depleted (not detected, below 1 μM), which  
339 are conditions that prevent dissolved Mn(II) oxidation (Stumm and Morgan 1996; Morgan 2005;  
340 Luther 2010). However, the mixing of cold oxygenated water with hot reducing waters rich in Fe<sup>2+</sup>  
341 and H<sub>2</sub>S produce a dynamic reaction zone that leads to reactive oxygen species formation as the  
342 direct reaction of Fe<sup>2+</sup> with O<sub>2</sub> is thermodynamically favorable but the reaction of Mn<sup>2+</sup> is not  
343 favorable (Luther, 2010). Shaw et al. (2021) demonstrated an oxidative pathway involving reactive  
344 oxygen species as H<sub>2</sub>O<sub>2</sub> was detected up to 6.2 μM. In particular, while overall oxidation by O<sub>2</sub> is  
345 faster for Fe(II) than for Mn(II) leading to O<sub>2</sub><sup>-</sup>, O<sub>2</sub><sup>-</sup> reacts faster with Mn(II) to produce H<sub>2</sub>O<sub>2</sub> by an  
346 order of magnitude (Rush and Bielski 1985; Barnese et al. 2012). Therefore, as for Fe(III) (Bennett  
347 et al. 2008) and Cu(II) (Sander et al. 2007), organic ligands stabilize dissolved manganese released  
348 by hydrothermal vents, in this case as a metastable Mn(III) complex. Overall, the sequence of  
349 reactions is given to form Mn(III) by the following equations (1-3):



353 Fe<sup>3+</sup> can also react with L to form Fe(III)-L as well as with H<sub>2</sub>S to reform Fe<sup>2+</sup>, and acts as a  
354 catalyzer of the Mn oxidation (Shaw et al, 2021).

355 Figure 5 shows dissolved Mn(II) removal in the concentrated plume as expected from previous  
356 studies (e.g. Lupton et al., 1980; Resing et al., 2015; Fitzsimmons et al., 2017) but this trend is  
357 observed only with one point, the less diluted one. Our dataset indicates that no Mn(III)-humic acid  
358 is formed in the concentrated plume which suggests the absence of direct Mn(II) oxidation and  
359 contrasts with the Mn(III)-humic acid production in the venting water. The removal could indeed  
360 be produced by adsorption onto particles or biological uptake.

361 The April 6 data show no temperature anomalies in agreement with no detection of Mn(III)-  
362 humic acid. However, the 5 nM total dissolved Mn we measured is much higher than the oceanic  
363 end member, indicating that at dilution above 20,000, the plume contains only dissolved Mn(II)  
364 and no Mn(III)-humic acid. Similar diluted plume water from the East Pacific Rise at 15°S showed  
365 a dissolved Mn concentration of 15 nM (Resing et al. 2015) and was about one month old according  
366 to radium isotopes (Kipp et al. 2018). Assuming a similar order of magnitude between East Pacific  
367 Rise at 15°S and at 9°50'N, we can roughly estimate that the April 6<sup>th</sup> data point with dissolved  
368 Mn(II) = 5 nM is about one month old. Thus, the Mn(III) stabilization by the humic ligand is  
369 transient, the Mn(III)-humic acid being removed after about a month in diluted plume as it is in the  
370 ocean water column (see §5.2.3).

371 To sum up, dissolved Mn(III) is produced in the venting plume due to partial dissolved Mn(II)  
372 oxidation when reactive oxygen species are produced; the dissolved Mn(III) is simultaneously  
373 stabilized by humic like materials. While transported away and progressively diluted (from 10 to  
374 10,000 fold) part of the dissolved Mn(II) pool seems to be removed, probably by adsorption onto  
375 particles, while dissolved Mn(III) stays in solution. Then, farther away, once the plume dilution  
376 exceeds 10,000, the particles are less concentrated and dissolved Mn(II) removal becomes  
377 ineffective (e.g. Mottl et al., 1995), whereas metastable Mn(III)-humic acid has reacted to form

378 stable dissolved Mn(II) or particulate Mn(IV) and is no longer detected. A key to this study was  
379 the use of a transponder system on the CTD rosette and on the basalt bottom to sample closer to  
380 vent sources so that the concentrated rising plume could be better sampled.



381

382

## Conclusion

383 We find significant concentrations of Mn(III) bound to humic acid-type ligands in the Pacific  
384 Margin, based on a decrease of the absorbance signal of the Mn-porphyrin complex after  
385 acidification and filtration. One third of our samples shows Mn(III)-humic acid occurrence, in  
386 particular in the oxic/anoxic transitions characterized by intense mixing, that happen in two oceanic  
387 environments, near the vent and in the oxygen minimum zone after the squall. In Shaw et al (2021),  
388 we showed that dissolved Mn(III) was produced in the venting water due to the formation of  
389 reactive oxygen species. Here, we show that Mn(III)-humic acid is conservative and stable in the  
390 concentrated plume while Mn(II) is removed, probably by adsorption. However, in the diluted  
391 plume all the Mn(III)-humic acid reacts with the ambient oceanic species and is not measurable. In  
392 the steady state water column, no Mn(III)-humic acid was observed, even across the oxygen  
393 minimum zone. However, a squall was enough to increase water mixing and stimulate redox  
394 reactions, which result in Mn(III)-humic acid formation. These results are in line with the  
395 hypothesis that wet Mn oxides deposition followed by reductive dissolution are an important  
396 dissolved Mn source for the oceanic Mn cycle. Such events would modify on a short term, less than  
397 a month, the biogeochemistry of the top oceanic layer that is not easily sampled by traditional  
398 cruises that spend a day per station.

## 399 Acknowledgements

400 This work was funded by grants from the Chemical Oceanography program (OCE-1558738 to  
401 GWL; OCE-1558692 to BMT) and the Marine Geology and Geophysics program (OCE-1558712  
402 to GWL) of the National Science Foundation. Thanks to the crew of the R/V *Atlantis* who made  
403 sampling for this research possible. The authors declare no conflict of interests.

## Bibliography

- 404
- 405 Babin, S. M., Carton J. A., Dickey T. D., and Wiggert J. D. 2004. Satellite evidence of hurricane-
- 406 induced phytoplankton blooms in an oceanic desert. *J. Geophys. Res. Oceans* **109**.
- 407 doi:10.1029/2003JC001938
- 408 Barnese, K., E. B. Gralla, J. S. Valentine, and D. E. Cabelli. 2012. Biologically relevant mechanism
- 409 for catalytic superoxide removal by simple manganese compounds. *Proc. Natl. Acad. Sci.*
- 410 **109**: 6892–6897. doi:10.1073/pnas.1203051109
- 411 Bartlett, R. J. 1981. Nonmicrobial Nitrite-to-Nitrate Transformation in Soils 1. *Soil Sci. Soc. Am.*
- 412 **J. 45**: 1054–1058. doi:10.2136/sssaj1981.03615995004500060009x
- 413 Bennett, S. A., E. P. Achterberg, D. P. Connelly, P. J. Statham, G. R. Fones, and C. R. German.
- 414 2008. The distribution and stabilisation of dissolved Fe in deep-sea hydrothermal plumes.
- 415 *Earth Planet. Sci. Lett.* **270**: 157–167. doi:10.1016/j.epsl.2008.01.048
- 416 Buck, C. S., A. Aguilar-Islas, C. Marsay, D. Kadko, and W. M. Landing. 2019. Trace element
- 417 concentrations, elemental ratios, and enrichment factors observed in aerosol samples
- 418 collected during the US GEOTRACES eastern Pacific Ocean transect (GP16). *Chem. Geol.*
- 419 **511**: 212–224. doi:10.1016/j.chemgeo.2019.01.002
- 420 Cole, S. T., C. Wortham, E. Kunze, and W. B. Owens. 2015. Eddy stirring and horizontal diffusivity
- 421 from Argo float observations: Geographic and depth variability: ARGO EDDY STIRRING
- 422 AND DIFFUSIVITY. *Geophys. Res. Lett.* **42**: 3989–3997. doi:10.1002/2015GL063827
- 423 Cowen, J. P., G. J. Massoth, and E. T. Baker. 1986. Bacterial scavenging of Mn and Fe in a mid-
- 424 to far-field hydrothermal particle plume. *Nature* **322**: 169–171. doi:10.1038/322169a0

425 Cutter, G. A., J. W. Moffett, M. C. Nielsdóttir, and V. Sanial. 2018. Multiple oxidation state trace  
426 elements in suboxic waters off Peru: In situ redox processes and advective/diffusive  
427 horizontal transport. *Mar. Chem.* **201**: 77–89. doi:10.1016/j.marchem.2018.01.003

428 Duckworth, O. W., and G. Sposito. 2007. Siderophore-promoted dissolution of synthetic and  
429 biogenic layer-type Mn oxides. *Chem. Geol.* **242**: 497–508.  
430 doi:10.1016/j.chemgeo.2007.05.007

431 Ehrlich, H. L. 1983. Manganese-Oxidizing Bacteria from a Hydrothermally Active Area on the  
432 Galapagos Rift. *Ecol. Bull.* 357–366.

433 Fitzsimmons, J. N., E. A. Boyle, and W. J. Jenkins. 2014. Distal transport of dissolved  
434 hydrothermal iron in the deep South Pacific Ocean. *Proc. Natl. Acad. Sci.* **111**: 16654–  
435 16661. doi:10.1073/pnas.1418778111

436 Fitzsimmons, J. N., S. G. John, C. M. Marsay, C. L. Hoffman, S. L. Nicholas, B. M. Toner, C. R.  
437 German, and R. M. Sherrell. 2017. Iron persistence in a distal hydrothermal plume  
438 supported by dissolved–particulate exchange. *Nat. Geosci.* **10**: 195–201.  
439 doi:10.1038/ngeo2900

440 Guieu, C., R. Duce, and R. Arimoto. 1994. Dissolved input of manganese to the ocean: Aerosol  
441 source. *J. Geophys. Res. Atmospheres* **99**: 18789–18800. doi:10.1029/94JD01120

442 Hartman, J. R., B. M. Foxman, and S. R. Cooper. 1984. Higher valent manganese chemistry.  
443 Synthetic, structural, and solution studies on [Mn (catecholate) <sub>3</sub>] <sup>n-</sup>(n= 2, 3) complexes.  
444 *Inorg. Chem.* **23**: 1381–1387.

445 Irving, H., and R. J. P. Williams. 1948. Order of stability of metal complexes. *Nature* **162**: 746–  
446 747.

447 Ishii, H., H. Koh, and K. Satoh. 1982. Spectrophotometric determination of manganese utilizing  
448 metal ion substitution in the cadmium- $\alpha$ ,  $\beta$ ,- $\gamma$ ,  $\delta$ -tetrakis (4-carboxyphenyl) porphine  
449 complex. *Anal. Chim. Acta* **136**: 347–352.

450 Johnson, K. S., K. H. Coale, W. M. Berelson, and R. M. Gordon. 1996. On the formation of the  
451 manganese maximum in the oxygen minimum. *Geochim. Cosmochim. Acta* **60**: 1291–  
452 1299.

453 Jones, M. R., G. W. Luther, and B. M. Tebo. 2020. Distribution and concentration of soluble  
454 manganese(II), soluble reactive Mn(III)-L, and particulate MnO<sub>2</sub> in the Northwest Atlantic  
455 Ocean. *Mar. Chem.* **226**: 103858. doi:10.1016/j.marchem.2020.103858

456 Jones, M. R., V. E. Oldham, G. W. Luther, A. Mucci, and B. M. Tebo. 2019. Distribution of  
457 desferrioxamine-B-extractable soluble manganese(III) and particulate MnO<sub>2</sub> in the St.  
458 Lawrence Estuary, Canada. *Mar. Chem.* **208**: 70–82. doi:10.1016/j.marchem.2018.11.005

459 Kessler, W. S. 2006. The circulation of the eastern tropical Pacific: A review. *Prog. Oceanogr.* **69**:  
460 181–217. doi:10.1016/j.pocean.2006.03.009

461 Kipp, L. E., V. Sanial, P. B. Henderson, P. van Beek, J.-L. Reyss, D. E. Hammond, W. S. Moore,  
462 and M. A. Charette. 2018. Radium isotopes as tracers of hydrothermal inputs and neutrally  
463 buoyant plume dynamics in the deep ocean. *Mar. Chem.* **201**: 51–65.  
464 doi:10.1016/j.marchem.2017.06.011

465 Klinkhammer, G., M. Bender, and R. F. Weiss. 1977. Hydrothermal manganese in the Galapagos  
466 Rift. *Nature* **269**: 319–320. doi:10.1038/269319a0

467 Klinkhammer, G. P., and M. L. Bender. 1980. The distribution of manganese in the Pacific Ocean.  
468 *Earth Planet. Sci. Lett.* **46**: 361–384.

469 Kostka, J. E., G. W. Luther, and K. H. Nealson. 1995. Chemical and biological reduction of  
470 Mn(III)-pyrophosphate complexes: Potential importance of dissolved Mn(III) as an  
471 environmental oxidant. *Geochim. Cosmochim. Acta* **59**: 885–894.

472 Lam, P. J., J.-M. Lee, M. I. Heller, S. Mehic, Y. Xiang, and N. R. Bates. 2018. Size-fractionated  
473 distributions of suspended particle concentration and major phase composition from the  
474 U.S. GEOTRACES Eastern Pacific Zonal Transect (GP16). *Mar. Chem.* **201**: 90–107.  
475 doi:10.1016/j.marchem.2017.08.013

476 Lang, S. Q., D. A. Butterfield, M. D. Lilley, H. Paul Johnson, and J. I. Hedges. 2006. Dissolved  
477 organic carbon in ridge-axis and ridge-flank hydrothermal systems. *Geochim. Cosmochim.*  
478 *Acta* **70**: 3830–3842. doi:10.1016/j.gca.2006.04.031

479 Lewis, B. L., and G. W. Luther III. 2000. Processes controlling the distribution and cycling of  
480 manganese in the oxygen minimum zone of the Arabian Sea. *Deep Sea Res. Part II Top.*  
481 *Stud. Oceanogr.* **47**: 1541–1561.

482 Lin, H., N. H. Szeinbaum, T. J. DiChristina, and M. Taillefert. 2012. Microbial Mn(IV) reduction  
483 requires an initial one-electron reductive solubilization step. *Geochim. Cosmochim. Acta*  
484 **99**: 179–192. doi:10.1016/j.gca.2012.09.020

485 Longnecker, K., S. M. Sievert, S. P. Sylva, J. S. Seewald, and E. B. Kujawinski. 2018. Dissolved  
486 organic carbon compounds in deep-sea hydrothermal vent fluids from the East Pacific Rise  
487 at 9°50'N. *Org. Geochem.* **125**: 41–49. doi:10.1016/j.orggeochem.2018.08.004

488 Lupton, J. E., G. P. Klinkhammer, W. R. Normark, R. Haymon, K. C. MacDonald, R. F. Weiss,  
489 and H. Craig. 1980. Helium-3 and manganese at the 21°N East Pacific Rise hydrothermal  
490 site. *Earth Planet. Sci. Lett.* **50**: 115–127. doi:10.1016/0012-821X(80)90123-5

491 Luther, G. W. 2005. Manganese(II) Oxidation and Mn(IV) Reduction in the Environment—Two  
492 One-Electron Transfer Steps Versus a Single Two-Electron Step. *Geomicrobiol. J.* **22**: 195–  
493 203. doi:10.1080/01490450590946022

494 Luther, G. W. 2010. The role of one-and two-electron transfer reactions in forming  
495 thermodynamically unstable intermediates as barriers in multi-electron redox reactions.  
496 *Aquat. Geochem.* **16**: 395–420.

497 Luther, G. W. 2021. Hydrothermal Vents Are a Source of Old Refractory Organic Carbon to the  
498 Deep Ocean. *Geophys. Res. Lett.* **48**: e2021GL094869. doi:10.1029/2021GL094869

499 Luther, G. W., A. S. Madison, A. Mucci, B. Sundby, and V. E. Oldham. 2015. A kinetic approach  
500 to assess the strengths of ligands bound to soluble Mn(III). *Mar. Chem.* **173**: 93–99.  
501 doi:10.1016/j.marchem.2014.09.006

502 Luther, G. W., B. Sundby, B. L. Lewis, P. J. Brendel, and N. Silverberg. 1997. Interactions of  
503 manganese with the nitrogen cycle: alternative pathways to dinitrogen. *Geochim.*  
504 *Cosmochim. Acta* **61**: 4043–4052.

505 Luther, G. W., A. Thibault de Chanvalon, V. E. Oldham, E. R. Estes, B. M. Tebo, and A. S.  
506 Madison. 2018. Reduction of Manganese Oxides: Thermodynamic, Kinetic and  
507 Mechanistic Considerations for One- Versus Two-Electron Transfer Steps. *Aquat.*  
508 *Geochem.* doi:10.1007/s10498-018-9342-1

509 Madison, A. S., B. M. Tebo, and G. W. Luther. 2011. Simultaneous determination of soluble  
510 manganese(III), manganese(II) and total manganese in natural (pore)waters. *Talanta* **84**:  
511 374–381. doi:10.1016/j.talanta.2011.01.025

512 Madison, A. S., B. M. Tebo, A. Mucci, B. Sundby, and G. W. Luther. 2013. Abundant porewater  
513 Mn (III) is a major component of the sedimentary redox system. *science* **341**: 875–878.

514 Mandernack, K. W., and B. M. Tebo. 1993. Manganese scavenging and oxidation at hydrothermal  
515 vents and in vents plumes. *Geochim. Cosmochim. Acta* **57**: 3907–3923.

516 Marsay, C. M., D. Kadko, W. M. Landing, and C. S. Buck. 2022. Bulk Aerosol Trace Element  
517 Concentrations and Deposition Fluxes During the U.S. GEOTRACES GP15 Pacific  
518 Meridional Transect. *Glob. Biogeochem. Cycles* **36**: e2021GB007122.  
519 doi:10.1029/2021GB007122

520 Martin, J. H., and G. A. Knauer. 1984. VERTEX: manganese transport through oxygen minima.  
521 *Earth Planet. Sci. Lett.* **67**: 35–47.

522 Martin, J. H., G. A. Knauer, and W. W. Broenkow. 1985. VERTEX: the lateral transport of  
523 manganese in the northeast Pacific. *Deep Sea Res. Part Oceanogr. Res. Pap.* **32**: 1405–1427.

524 McManus, J., W. M. Berelson, S. Severmann, K. S. Johnson, D. E. Hammond, M. Roy, and K. H.  
525 Coale. 2012. Benthic manganese fluxes along the Oregon–California continental shelf and  
526 slope. *Cont. Shelf Res.* **43**: 71–85.

527 Mendez, J., C. Guieu, and J. Adkins. 2010. Atmospheric input of manganese and iron to the ocean:  
528 Seawater dissolution experiments with Saharan and North American dusts. *Mar. Chem.*  
529 **120**: 34–43. doi:10.1016/j.marchem.2008.08.006

530 Morgan, J. J. 2005. Kinetics of reaction between O<sub>2</sub> and Mn(II) species in aqueous solutions.  
531 *Geochim. Cosmochim. Acta* **69**: 35–48. doi:10.1016/j.gca.2004.06.013

532 Mottl, M. J., F. J. Sansone, C. Geoffrey Wheat, J. A. Resing, E. T. Baker, and J. E. Lupton. 1995.  
533 Manganese and methane in hydrothermal plumes along the East Pacific Rise, 8°40' to  
534 11°50'N. *Geochim. Cosmochim. Acta* **59**: 4147–4165. doi:10.1016/0016-7037(95)00245-  
535 U

536 Murray, J. W., B. Spell, and B. Paul. 1983. The contrasting geochemistry of manganese and  
537 chromium in the eastern tropical Pacific Ocean, p. 643–669. *In* Trace metals in sea water.  
538 Springer.

539 Oldham, V. E., M. R. Jones, B. M. Tebo, and G. W. Luther. 2017a. Oxidative and reductive  
540 processes contributing to manganese cycling at oxic-anoxic interfaces. *Mar. Chem.* **195**:  
541 122–128. doi:10.1016/j.marchem.2017.06.002

542 Oldham, V. E., C. H. Lamborg, and C. M. Hansel. 2020. The Spatial and Temporal Variability of  
543 Mn Speciation in the Coastal Northwest Atlantic Ocean. *J. Geophys. Res. Oceans* **125**.  
544 doi:10.1029/2019JC015167

545 Oldham, V. E., A. Mucci, B. M. Tebo, and G. W. Luther. 2017b. Soluble Mn(III)–L complexes are  
546 abundant in oxygenated waters and stabilized by humic ligands. *Geochim. Cosmochim.*  
547 *Acta* **199**: 238–246. doi:10.1016/j.gca.2016.11.043

548 Perez-Benito, J. F. 2002. Reduction of Colloidal Manganese Dioxide by Manganese(II). *J. Colloid*  
549 *Interface Sci.* **248**: 130–135. doi:10.1006/jcis.2001.8145

550 Peters, B. D., W. J. Jenkins, J. H. Swift, C. R. German, J. W. Moffett, G. A. Cutter, M. A.  
551 Brzezinski, and K. L. Casciotti. 2018. Water mass analysis of the 2013 US GEOTRACES  
552 eastern Pacific zonal transect (GP16). *Mar. Chem.* **201**: 6–19.  
553 doi:10.1016/j.marchem.2017.09.007

554 Resing, J. A., P. N. Sedwick, C. R. German, W. J. Jenkins, J. W. Moffett, B. M. Sohst, and A.  
555 Tagliabue. 2015. Basin-scale transport of hydrothermal dissolved metals across the South  
556 Pacific Ocean. *Nature* **523**: 200–203. doi:10.1038/nature14577

557 Ruppel, D. T., S. C. Dexter, and G. W. Luther. 2001. Role of Manganese Dioxide in Corrosion in  
558 the Presence of Natural Biofilms. *CORROSION* **57**: 863–873. doi:10.5006/1.3290313



559 Rush, J. D., and B. H. J. Bielski. 1985. Pulse radiolytic studies of the reaction of  
560 perhydroxyl/superoxide O<sub>2</sub><sup>-</sup> with iron(II)/iron(III) ions. The reactivity of HO<sub>2</sub>/O<sub>2</sub><sup>-</sup> with  
561 ferric ions and its implication on the occurrence of the Haber-Weiss reaction. 5.

562 Sander, S. G., A. Koschinsky, G. Massoth, M. Stott, and K. A. Hunter. 2007. Organic complexation  
563 of copper in deep-sea hydrothermal vent systems. *Environ. Chem.* **4**: 81–89.  
564 doi:10.1071/EN06086

565 Sanial, V., L. E. Kipp, P. B. Henderson, and others. 2017. Radium-228 as a tracer of dissolved trace  
566 element inputs from the Peruvian continental margin. *Mar. Chem.*  
567 doi:10.1016/j.marchem.2017.05.008

568 Shaw, T. J., G. W. Luther, R. Rosas, and others. 2021. Fe-catalyzed sulfide oxidation in  
569 hydrothermal plumes is a source of reactive oxygen species to the ocean. *Proc. Natl. Acad.*  
570 *Sci.* **118**: e2026654118. doi:10.1073/pnas.2026654118

571 Stone, A. T. 1987. Reductive Dissolution of Manganese(III/IV) Oxides by Substituted Phenols.  
572 *Environ. Sci. Technol.* **21**: 979–988. doi:10.1021/es50001a011

573 Stone, A. T., and J. J. Morgan. 1984. Reduction and dissolution of manganese (III) and manganese  
574 (IV) oxides by organics. 1. Reaction with hydroquinone. *Environ. Sci. Technol.* **18**: 450–  
575 456.

576 Stumm, W., and J. J. Morgan. 1996. *Aquatic chemistry: chemical equilibria and rates in natural*  
577 *waters*, John Wiley & Sons.

578 Sunda, W. G., and S. A. Huntsman. 1988. Effect of sunlight on redox cycles of manganese in the  
579 southwestern Sargasso Sea. *Deep Sea Res. Part Oceanogr. Res. Pap.* **35**: 1297–1317.  
580 doi:10.1016/0198-0149(88)90084-2

581 Sunda, W. G., and S. A. Huntsman. 1990. Diel cycles in microbial manganese oxidation and  
582 manganese redox speciation in coastal waters of the Bahama Islands. *Limnol. Oceanogr.*  
583 **35**: 325–338. doi:10.4319/lo.1990.35.2.0325

584 Sunda, W. G., S. A. Huntsman, and G. R. Harvey. 1983. Photoreduction of manganese oxides in  
585 seawater and its geochemical and biological implications. *Nature* **301**: 234–236.  
586 doi:10.1038/301234a0

587 Thibault de Chanvalon, A., and G. W. Luther. 2019. Mn speciation at nanomolar concentrations  
588 with a porphyrin competitive ligand and UV–vis measurements. *Talanta* **200**: 15–21.  
589 doi:10.1016/j.talanta.2019.02.069

590 Trouwborst, R. E., B. G. Clement, B. M. Tebo, B. T. Glazer, and G. W. Luther. 2006. Soluble  
591 Mn(III) in Suboxic Zones. *Science* **313**: 1955–1957. doi:10.1126/science.1132876

592 Van Cappellen, P., and Y. Wang. 1996. Cycling of iron and manganese in surface sediments; a  
593 general theory for the coupled transport and reaction of carbon, oxygen, nitrogen, sulfur,  
594 iron, and manganese. *Am. J. Sci.* **296**: 197–243.

595 Vedamati, J., C. Chan, and J. W. Moffett. 2015. Distribution of dissolved manganese in the  
596 Peruvian Upwelling and Oxygen Minimum Zone. *Geochim. Cosmochim. Acta* **156**: 222–  
597 240. doi:10.1016/j.gca.2014.10.026

598 Yakushev, E., S. Pakhomova, K. Sørensen, and J. Skei. 2009. Importance of the different  
599 manganese species in the formation of water column redox zones: Observations and  
600 modeling. *Mar. Chem.* **117**: 59–70. doi:10.1016/j.marchem.2009.09.007

601

602

## Supporting Information

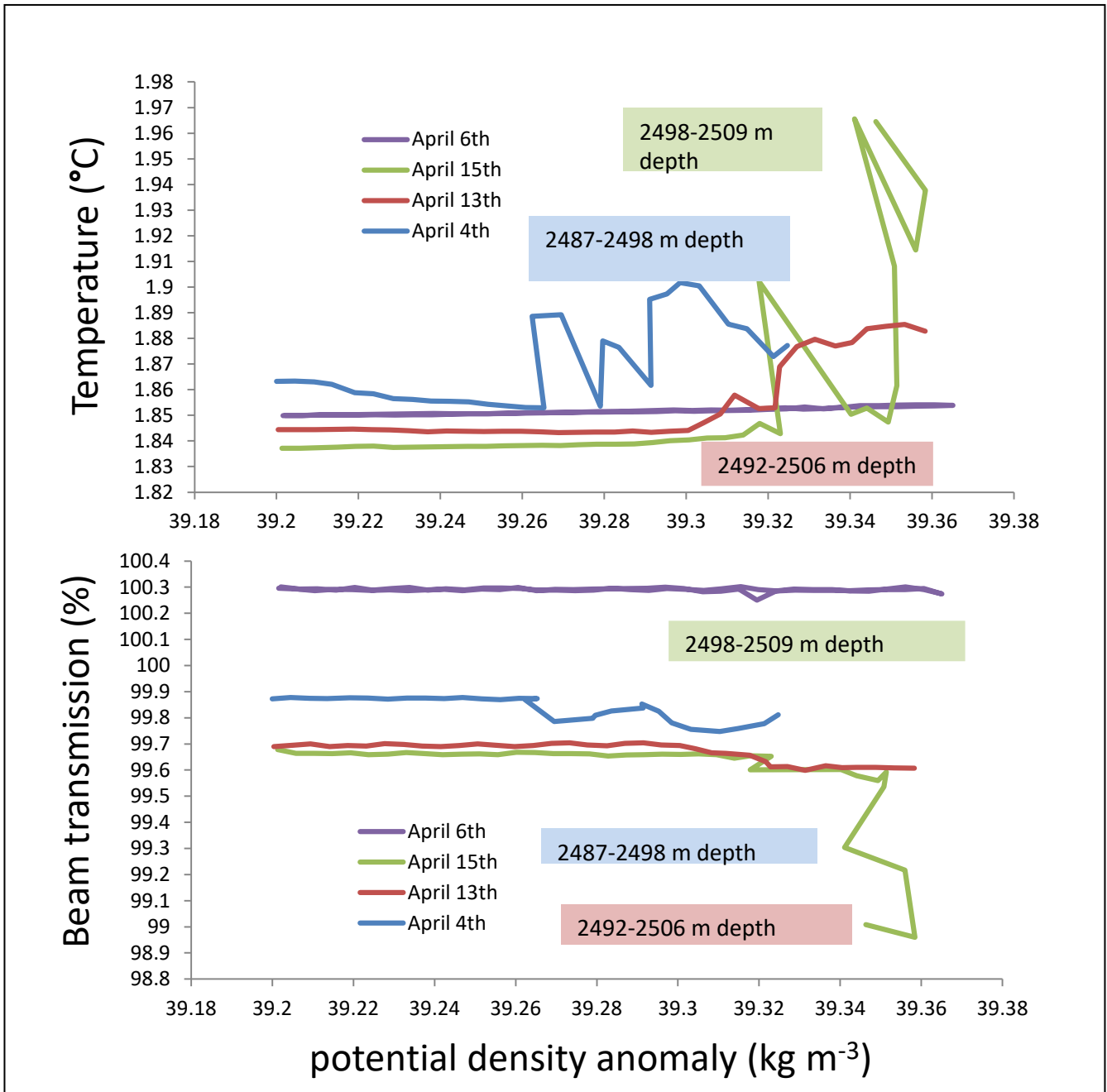
603 **Supporting Information, Table S1: Dataset of Mn concentration and speciation.**604 **NH<sub>2</sub>OH reduced method was not processed on 4/13 and 4/15.**

Date	Depth (m)	$\sigma_\theta$	"heated only" method	"NH <sub>2</sub> OH reduced" method	"HA removed" method	% Mn(III)-humic acid		
April 4 <sup>th</sup>	1	21.0	2.8 ± 0.5	3.6 ± 0.5	2.8 ± 0.5	-	±	-
April 4 <sup>th</sup>	30	21.4	2.9 ± 0.5	3.0 ± 0.4	3.1 ± 0.7	-	±	-
April 4 <sup>th</sup>	70	23.0	3.2 ± 0.6	3.7 ± 0.5	3.2 ± 1.5	-	±	-
April 4 <sup>th</sup>	85	24.8	5.4 ± 1	5.9 ± 1.9	5.6 ± 0.7	-	±	-
April 4 <sup>th</sup>	98	26.1	3.4 ± 0.4	3.5 ± 0.7	2.5 ± 0.5	-	±	-
April 4 <sup>th</sup>	260	27.7	2.7 ± 0.5	3.0 ± 0.5	2.1 ± 0.6	-	±	-
April 4 <sup>th</sup>	500	29.2	4.4 ± 0.9	4.6 ± 0.5	3.9 ± 0.6	-	±	-
April 4 <sup>th</sup>	615	29.9	4.1 ± 0.9	4.0 ± 0.4	3.3 ± 0.5	-	±	-
April 4 <sup>th</sup>	1400	34.1	2.8 ± 0.4	3.1 ± 0.6	2.4 ± 0.8	-	±	-
April 4 <sup>th</sup>	2000	37.0	2.5 ± 0.4	3.0 ± 0.4	2.7 ± 0.8	-	±	-
April 4 <sup>th</sup>	2494	39.3	28.2 ± 1.9	26.6 ± 1.4	10.2 ± 5.0	64.0 ± 19.0		
April 6 <sup>th</sup>	1	21.2	2.7 ± 0.2	2.8 ± 0.3	2.3 ± 0.3	-	±	-
April 6 <sup>th</sup>	30	21.4	2.6 ± 0.2	2.3 ± 0.3	2.3 ± 0.3	-	±	-
April 6 <sup>th</sup>	65	23.0	2.7 ± 0.2	2.6 ± 0.3	2.6 ± 0.3	-	±	-
April 6 <sup>th</sup>	70	23.9	3.7 ± 0.3	3.6 ± 0.4	3.7 ± 0.3	-	±	-
April 6 <sup>th</sup>	80	25.0	2.5 ± 0.3	2.2 ± 0.3	2.7 ± 0.4	-	±	-
April 6 <sup>th</sup>	90	25.6	2.9 ± 0.8	3.0 ± 0.3	3.3 ± 0.2	-	±	-
April 6 <sup>th</sup>	100	26.0	3.0 ± 0.3	2.4 ± 0.4	3.5 ± 0.3	-	±	-
April 6 <sup>th</sup>	110	26.4	3.0 ± 0.2	2.8 ± 0.3	3.4 ± 0.2	-	±	-
April 6 <sup>th</sup>	260	27.8	2.4 ± 0.6	2.0 ± 0.4	1.3 ± 0.5	-	±	-
April 6 <sup>th</sup>	400	28.6	3.7 ± 0.2	3.6 ± 0.3	3.3 ± 0.3	-	±	-
April 6 <sup>th</sup>	615	30.0	3.7 ± 0.4	3.2 ± 0.3	3.2 ± 0.5	-	±	-
April 6 <sup>th</sup>	1500	34.6	2.4 ± 0.2	3.0 ± 1.7	2.0 ± 0.5	-	±	-
April 6 <sup>th</sup>	2500	39.3	5.1 ± 0.4	5.8 ± 0.4	5.7 ± 0.3	-	±	-
April 13 <sup>th</sup>	30	21.2	5.1 ± 0.3		5.1 ± 0.6	-	±	-
April 13 <sup>th</sup>	60	22.1	4.9 ± 0.3		4.8 ± 0.4	-	±	-
April 13 <sup>th</sup>	73	23.4	8.4 ± 0.5		6.8 ± 0.5	19.3 ± 8.0		
April 13 <sup>th</sup>	80	24.4	5.3 ± 0.4		5.8 ± 0.6	-	±	-
April 13 <sup>th</sup>	86	26.9	5.3 ± 0.3		3.5 ± 0.3	33.5 ± 8.0		
April 13 <sup>th</sup>	140	27.9	14.2 ± 0.9		7.6 ± 0.8	46.6 ± 8.3		

April 13 <sup>th</sup>	400	28.9	8.2 ± 0.5	4.1 ± 1.5	49.7 ± 19.5
April 13 <sup>th</sup>	530	29.9	5.5 ± 0.5	4.4 ± 0.4	20.0 ± 11.6
April 13 <sup>th</sup>	700	30.9	3.6 ± 0.4	3.2 ± 0.3	- ± -
April 13 <sup>th</sup>	1500	31.9	2.4 ± 0.4	2.7 ± 0.4	- ± -
April 13 <sup>th</sup>	2000	32.9	3.5 ± 0.7	2.6 ± 0.4	- ± -
April 13 <sup>th</sup>	2500	33.9	20.7 ± 1.1	12.5 ± 0.7	39.7 ± 6.0
April 15 <sup>th</sup>	50	21.8	4.7 ± 1.1	4.5 ± 0.7	- ± -
April 15 <sup>th</sup>	60	22.3	5.2 ± 0.9	3.7 ± 0.7	- ± -
April 15 <sup>th</sup>	70	23.2	5.7 ± 0.5	3.5 ± 0.8	37.2 ± 17.1
April 15 <sup>th</sup>	76	23.6	6.0 ± 0.4	3.1 ± 0.9	47.7 ± 16.1
April 15 <sup>th</sup>	82.5	24.2	5.5 ± 0.6	4.1 ± 0.4	24.6 ± 13.2
April 15 <sup>th</sup>	110	26.3	6.9 ± 0.5	4.7 ± 0.8	32.7 ± 12.9
April 15 <sup>th</sup>	680	30.3	10.2 ± 1.4	8.1 ± 0.6	20.3 ± 15.3
April 15 <sup>th</sup>	1500	34.6	2.2 ± 0.5	2.1 ± 0.6	- ± -
April 15 <sup>th</sup>	2500	39.3	134.4 ± 7.5	85.1 ± 4.3	36.7 ± 6.4

605

606 Supporting Information, Figure S1: Temperature and beam transmission in the  
607 deeper meters from CTD casts.



608